

Kinematic Properties and Stellar Populations of Faint Early-Type Galaxies. I. Velocity Dispersion Measurements of Central Coma Galaxies

A. Matković¹* and R. Guzmán¹

¹Department of Astronomy, University of Florida, P.O. Box 112055, Gainesville, FL 32611, USA

Accepted 2005 June 16. Received 2004 November 25

ABSTRACT

We present velocity dispersion measurements for 69 faint early-type galaxies in the core of the Coma cluster, spanning $-22.0 \lesssim M_R \lesssim -17.5$ mag. We examine the $L - \sigma$ relation for our sample and compare it to that of bright ellipticals from the literature. The distribution of the faint early-type galaxies in the $L - \sigma$ plane follows the relation $L \propto \sigma^{2.01 \pm 0.36}$, which is significantly shallower from $L \propto \sigma^4$ as defined for the bright ellipticals. While increased rotational support for fainter early-type galaxies could account for some of the difference in slope, we show that it cannot explain it. We also investigate the Colour– σ relation for our Coma galaxies. Using the scatter in this relation, we constrain the range of galaxy ages as a function of their formation epoch for different formation scenarios. Assuming a strong coordination in the formation epoch of faint early-type systems in Coma, we find that most had to be formed at least 6 Gyrs ago and over a short 1 Gyr period.

Key words: galaxies: dwarf — galaxies: elliptical — galaxies: clusters: individual (Coma) — galaxies: kinematics — galaxies: velocity dispersions galaxies: formation.

1 INTRODUCTION

Dwarf elliptical galaxies (dEs) are low luminosity spheroidal systems with $M_B > -18$ mag (Sandage & Binggeli 1984) that have a low surface brightnesses, $\mu_{e,V} > 22$ mag arcsec $^{-2}$ (Ferguson & Binggeli 1994). Over the past two decades there has been considerable interest in studying dEs, despite the difficulty associated with observing these objects. In particular, there has been a number of extensive photometric studies that have concentrated on comparing dEs to the bright elliptical galaxies with $M_B \leq -20.50$ mag (Graham & Guzmán 2003). Two main arguments support the hypothesis that they are structurally distinct classes.

Firstly, many authors in the past argued that de Vaucouleur's $R^{1/4}$ law (de Vaucouleurs 1948) best fits the light profiles of bright Es. Meanwhile, Faber & Lyn (1983) and Binggeli, Sandage & Tarenghi (1984) showed that an exponential profile describes dwarf ellipticals. Secondly, as Kormendy (1985) notes, dEs and bright Es fall almost perpendicular to each other in the effective surface brightness–luminosity plot, $\mu_e - L$ and are clearly different in the luminosity–central surface brightness, $L - \mu_0$, plot. Further-

more, dEs and bright Es follow a different $\mu_e - R_e$ relation (e.g. Wirth & Gallagher 1984; Capaccioli, Caon & C'Onofrio 1992).

More evidence to strengthen the proposed dichotomy exists. Dwarf ellipticals seem to lie off the Fundamental Plane, the relation between the surface brightness at the effective radius, μ_e , effective half-light radius, R_e , and the velocity dispersion, σ (Bender, Burstein, & Faber 1992; de Carvalho, & Djorgovski 1992; Peterson, & Caldwell 1993). This disparity has been interpreted as a difference in the formation mechanism for dwarf and bright Es.

Nonetheless, there are many studies arguing for continuity in the dwarf-bright family. Just to mention a few: Caldwell 1983; Caldwell 1987; Caldwell & Bothun 1987; Ferguson & Sandage 1988; Hudson *et al.* 1997; Jerjen & Binggeli 1997; Jerjen, Binggeli, & Freeman 2000; and Karachentsev, *et al.* 1995. Some of these studies show that dEs exhibit the same central surface brightness and absolute magnitude relation as bright Es. Caldwell (1983) also pointed out that a continuous trend exists between colour and luminosity, while Caldwell & Bothun (1987) show the same continuity for the luminosity–metallicity relation.

Graham & Guzmán (2003; hereafter GG03)(see also Guzmán *et al.* 2003) offer a possible resolution of the dif-

* E-mail: matkovic@astro.ufl.edu (AM)

fering views. They point out that the dichotomy in the luminosity–effective surface brightness relation, $M_B - \mu_e$, and the luminosity–effective radius relation, $M_B - R_e$, is a direct consequence of the linear relations between the luminosity, the central surface brightness, μ_0 , and the light profile shape, n . Furthermore, they argue that dEs and intermediate luminosity ellipticals follow a continuous sequence up to $M_B \sim -20.5$ mag. At this point bright ellipticals start showing evidence of evacuated cores, possibly coalescing black holes, causing their central surface brightness to decrease with increasing luminosity (GG03; Graham 2004 and references therein). The most massive Es may thus be the exception and not the rule to the empirical correlations defined by early-type galaxies that include the low luminosity galaxies and range over ~ 8 magnitudes (see GG03).

Up until the past couple of years most information on spectroscopic properties of dEs came from their line strength indices (Held & Mould 1994; Gorgas *et al.* 1997; Mobasher *et al.* 2002; Moore *et al.* 2002), and a handful of velocity dispersion measurements. Although more difficult to obtain due to low surface brightness of these objects, the number of papers in the literature which include velocity dispersion measurements of dEs in different clusters has increased (Bender & Nieto 1990; Brodie & Huchra 1991; Held *et al.* 1992; Bender, Burstein, & Faber 1992; Peterson & Caldwell 1993; Bernardi *et al.* 1998; Melhert *et al.* 2002; Hudson *et al.* 2001; De Rijcke *et al.* 2001; Simien & Prugniel 2002; Pedraz *et al.* 2002; Moore, Lucey, Kuntschner, & Colless 2002 (hereafter MLKC02); Geha, Guhathakurta, & van der Marel 2002, 2003; Guzmán *et al.* 2003; Bernardi *et al.* 2003; Smith *et al.* 2004, van Zee, Skillman, & Haynes 2004; De Rijcke *et al.* 2004). The NOAO Fundamental Plane survey (NFPS) of Smith *et al.* 2004 is the largest compilation including velocity dispersion measurements in low-redshift galaxy clusters up to date. Our Coma sample, although significantly smaller than that of the NFPS is complementary to this study. It includes a statistically representative sample of faint early-type galaxies in different environments within a cluster. Such sample is essential for testing current ideas on the formation and evolution of dEs.

Via recent studies, dEs have also been linked to the Butcher–Oemler effect (Butcher, & Oemler 1978; Butcher, & Oemler 1984). Observations of distant clusters reveal the existence of numerous star-forming, low-mass ‘blue disk’ galaxies in clusters at $z \sim 0.4$. These galaxies, as shown by HST, are distorted small spirals which have disappeared from the present day clusters. The fate of these galaxies remains one of the most important unanswered questions in modern cosmology. The ‘galaxy harassment’ model Moore, Lake & Katz (1996; 1998) explains how the dwarf spiral galaxies in clusters may evolve into today’s population of cluster dEs due to encounters with brighter galaxies and the cluster tidal field. The galaxy harassment model predicts differences in the properties of dEs located in the inner, high density, and outer, low density, regions of the clusters.

This is the first paper of a series in which we will characterise the kinematics and stellar populations of dEs and other low luminosity early-type galaxies as a function of the environment. Given the difficulty in distinguishing between dEs, dS0s, and dwarf spirals in Coma from ground-based images, we refer to all these objects as ‘early-type’ galaxies. For convenience, we define ‘faint’ early-type galaxies as

those with $M_B > -20.50$ mag, and the ‘bright’ ellipticals with $M_B \leq -20.50$ mag. Here we describe spectroscopic observations and velocity dispersion (σ) measurements of 69 faint early-type galaxies in the central $30' \times 30'$ region of the Coma cluster. We investigate whether these galaxies follow the luminosity–velocity dispersion ($L - \sigma$) relation derived for bright ellipticals, and discuss the constraints on their formation epochs provided by the colour– σ ($C - \sigma$) relation. In future papers, we will test the implications of the ‘galaxy harassment’ scenario by comparing the internal kinematics and stellar populations of the early-type galaxies in the core and the outskirts of the Coma cluster. Section 2 describes the photometric and spectroscopic observations of our sample galaxies, including the sample selection. In Section 3, we describe the data reduction technique and the velocity dispersion measurements. We investigate the $L - \sigma$ relation in Section 4, and the $C - \sigma$ relation in Section 5. A summary of our results is provided in Section 6.

2 OBSERVATIONS

2.1 Sample Selection

The selection of faint early-type galaxies in the Coma cluster was done using the photometry in U , B and R bands. We obtained the images with the WIYN/MiniMo and INT/Wide Field Camera. To select the faint early-type galaxy candidates in the central $30' \times 30'$ region of the Coma cluster we used the $B - R$ vs. B colour-magnitude plane. We applied an absolute luminosity cutoff at $M_B \geq -17.3$ mag (Ferguson, & Binggeli 1994; corresponding to apparent $B \gtrsim 17.5$ mag at the distance of the Coma cluster¹). To minimize contamination at the faint end by the background field disk galaxies at $z < 0.2$, we applied another cutoff using the $(U - B)$ vs. $(B - R)$ colour-colour diagram at $0.2 < (U - B) < 0.6$ mag, and $1.3 < (B - R) < 1.5$ mag.

2.2 Spectroscopic Observations

We observed the Coma cluster faint early-type galaxies during 1998 May 23–26, and 1999 May 14–19 on the 3.5 m WIYN telescope at Kitt Peak National Observatory with the multi-fibre spectrograph HYDRA. We used the 600 l mm⁻¹ grating in the 2nd order, and the blue fibre cable, which we chose for its transmission at the desired wavelengths. The selected grating allowed us to observe in the wavelength range of $\Delta\lambda = 4120 - 5600 \text{ \AA}$, which is optimal for discerning some of the most prominent absorption features of the faint early-type galaxies including molecular G-band, $H\gamma$, $H\beta$, Mg_2 , and $Fe\lambda 5350$. With this setup we achieved the dispersion of $\sim 0.705 \text{ \AA px}^{-1}$, while our instrumental resolution of $\text{FWHM} = 1.91 \text{ \AA}$ allowed us to detect velocity dispersions down to 35 km s^{-1} . This is assuming that we can measure velocity dispersions up to 30 percent better than the instrumental resolution for galaxies with $\text{SNR} > 15$.

The HYDRA multi-fibre spectrograph has ~ 100 fibres

¹ Throughout the paper we use $H_0 = 70 \text{ km s}^{-1} \text{ Mpc}^{-1}$, and a distance modulus for Coma cluster of 35.078, ($d = 99 \text{ Mpc}$).

each with $3''$ diameter. Thus, it is well suited for the detection of the faint early-type galaxies, which typically have a half light radius of $\sim 2''$ at the distance of Coma (GG03). We observed ~ 45 galaxies and ~ 45 adjacent sky spectra for each HYDRA setup. The galaxy sample was divided into 3 different groups depending on the exposure times to achieve $\text{SNR} \geq 15$. We observed the brightest galaxies $b_j \leq 17.5$ mag for a total integration time of 4 hours, objects with $17.50 < b_j \leq 18.5$ mag for 8 hours, and the faintest objects $b_j > 18.5$ mag for 16 hours. In addition, we obtained spectra of template stars representative of the prevailing stellar-population of dEs, primarily G and K-type stars. The sample also included ~ 30 bright elliptical galaxies observed in previous studies in order to assess any systematic effects. Sample spectra of 4 galaxies with different luminosities and SNR are given in Figure 1. All the candidates had enough signal for radial velocity measurements from which we conclude that 100 percent have the range of recession velocities of $4,000\text{--}10,000 \text{ km s}^{-1}$, consistent with membership in the Coma cluster (Colless & Dunn 1996).

3 DATA REDUCTION AND MEASUREMENTS

3.1 Basic Data Reduction

We used the basic and multi-fibre spectral reduction tasks within IRAF² to reduce our observations. The data was first trimmed accordingly and corrected for the overscan region. We removed the cosmic rays with FIGARO within the STARLINK software program. For the remaining reduction we used the ‘dohydra’ task within IRAF, which provided: aperture identification; tracing of the apertures; flat field correction for the pixel to pixel sensitivity and the different throughput from fibre to fibre; removal of internal reflections within the spectrograph (scattered light); the wavelength calibration; and the sky subtraction. The largest rms for the wavelength calibration was 0.02 \AA .

3.2 Velocity Dispersion and Radial Velocity Measurements

Velocity dispersions, σ , were measured from galaxy spectra with the software REDUCEME (Cardiel 1999). The program implements the Fourier quotient method (described by González-González 1993), originally introduced by Sargent *et al.* (1977), to measure the velocity dispersions. The Fourier quotient method assumes that observed galaxy spectra can be described as a convolution between the spectral characteristics of the stellar population, the broadening function, and the effective response function of the instrument. Using an initial guess of the velocity dispersion, the program calculates a broadening function described by the dispersion relation and models a galaxy spectrum as a convolution of the broadening function and an optimal stellar synthesis spectrum. This template for the galaxy is produced

² Image Reduction and Analysis Facility. Distributed by the National Optical Astronomy Observatories, which is operated by AURA (Association of Universities for Research in Astronomy, Inc) under cooperative agreement with the National Science Foundation.

by combination of the different star templates. Via χ^2 minimization between the galaxy and the model spectra, the best value of the velocity dispersion for the broadening function is determined.

We tested the stability of the software for a range of values of the involved parameters. The only difference in σ measurements occurred when we changed the wavelength range used to calculate the velocity dispersions and when we altered the tapering fraction. The measured velocity dispersion varied by 10 percent with the choice of the spectral region, and up to 20 percent for the faintest galaxies when varying the tapering fractions. We conducted a set of tests altering either the tapering fraction for a specific wavelength range, or the wavelength range for a specific tapering fraction. We found that the most stable solutions occurred for a tapering fraction of 0.25 and when we trimmed the spectra at the edges. We chose to trim the spectra by preserving the largest rest frame wavelength range possible: $4150 - 5400 \text{ \AA}$.

3.3 Uncertainty Measurements

We estimated the uncertainties in velocity dispersion measurements by the ‘bootstrapping’ technique implemented by J. Gorgas (private communication) within the REDUCEME software. Assuming that the noise in the galaxy spectrum is dominated by Poisson noise, the program uses Monte-Carlo realizations to produce simulated galaxy spectra with similar SNR to the original galaxy. For each galaxy we ran 50 simulations, after confirming that the results were the same for 100 simulations. The program then measures the velocity dispersion of each simulated galaxy and via χ^2 minimization estimates the error in the velocity dispersion measurements, which also accounts for the template mismatch.

We have checked internally and externally for systematical offsets in the velocity dispersion measurements in our sample of the core faint early-type galaxies. The external check consisted of comparing our measurements with those comparable in SNR and resolution in the literature, (MLKC02 and NFPS). Figure 2 shows the comparison of σ measurements and includes the uncertainty in the $\sigma/\sigma_{\text{Lit}}$. This plot shows no systematic offsets between our and the two literature samples. Furthermore, the median of the comparison, 1.01, and the rms scatter of the points, 0.10, indicate that our σ measurements are in good agreement with those of both NFPS (open triangles) and MLKC02 (solid triangles). We also note that some galaxies seem to be inconsistent with the average value when taking their uncertainties into account. This would imply that the uncertainties in the σ measurements are possibly underestimated. However, it is not possible to determine whether it is the literature, ours, or both uncertainties that are underestimated.

The internal check was done in the same way as the external, except that in this case σ was measured using only half of their exposures in our own data. We found no inconsistencies in the σ measurements nor their error measurements for our sample of faint early-type galaxies, but the error measurements for our bright ellipticals were, on average, underestimated by 30 percent. We have therefore increased the uncertainties of the bright Es by 30 percent.

In addition, our analysis excludes galaxies with SNR

< 15, since below this value the fit of the model spectra to the galaxy was uncertain. We also investigate the effects noise has on the velocity dispersion measurements. The following method closely resembles the analysis of Jørgensen, Franx & Kjærgaard (1995; hereafter JFK95). We selected a template star that best fits a typical galaxy with a high SNR, and broadened it by convolving it by Gaussians with σ ranging from 35 to 100 km s $^{-1}$. Different amounts of noise were added to each spectra so the SNR would yield values ranging 10–50. The unaltered spectra of the star was used as a template, while we measured the velocity dispersion of the broadened and lower SNR spectra. The final σ was derived after 1000 simulations using the bootstrapping method. Figure 3 shows the percentage difference between the 'galaxy' spectra (template spectra broadened to 50 km s $^{-1}$) and the observed σ , i.e. the same broadened galaxy with different amount of noise. All our simulated spectra have a slightly overestimated measurement of the velocity dispersion. The effect is larger for galaxies with a smaller velocity dispersion. For example, a galaxy with $\sigma = 35$ km s $^{-1}$ and SNR of 15 has σ overestimated by ~ 6 percent. JFK95 find that a galaxy with $\sigma = 65$ km s $^{-1}$ is overestimated by ~ 4 percent, and a galaxy with $\sigma = 100$ km s $^{-1}$ by ~ 1 percent which is in good agreement with our measurements. We chose not to correct for this systematic effect since it is significantly smaller than the uncertainties in the σ measurements for majority of the galaxies in our sample. Implications of this effect on the $L - \sigma$ relation are discussed in section 5.

4 RESULTS

The σ and radial velocity measurements for 87 early-type galaxies we observed in the Coma cluster are presented in Table 1. For the following analysis we only used 72 objects with SNR ≥ 15 . We classify galaxies with $M_R \leq -22.17$ mag as bright Es. Our sample includes 69 galaxies with $M_R > -22.17$ mag classified here as faint early-type galaxies and 3 bright Es. We include other samples from the literature with σ measurements and plot the galaxies in diagnostic diagrams to characterize their kinematic properties.

In Figure 4 (left) we show the $L - \sigma$ relation including galaxies with σ measurements from MLKC02, Hudson *et al.* (2001), EFAR (Colless *et al.* 2001), and our sample. The total number of galaxies is 167, where 24 galaxies are classified as bright Es. In case of multiple σ measurements from the literature, we used a minimum variance weighted average of velocity dispersions and calculated the error in the weighted average. When those galaxies were in common with our sample, we used the same process but adopted the symbol used for this paper (triangles) in the figure. Table 1 lists the σ values measured in our sample.

We have derived the photometry in M_R from Gutiérrez *et al.* (2004) for the MLKC02 and our sample, while the other catalogues included their own photometry. We averaged the actual luminosities for galaxies with multiple photometry. The uncertainty in the average of the magnitudes was 0.015 mag, except for 3 galaxies, which we excluded from the sample since their uncertainty was large and most likely due to a catalogue mismatch. Out of our sample of 72 galaxies with σ measurements, 17 were not in the Gutierrez list. In this case we have derived R (Johnson filter) by using the

b_j magnitudes listed in the GMP catalogue. We used a least squares fit to objects that had both b_j and R and obtained the transformation $R = (1.050 \pm 0.030)b_j - 2.422 \pm 0.529$ between these two magnitudes.

The $L - \sigma$ relation in Figure 4 (left) exhibits a curvature or a change of slope. To allow for a comparison with earlier studies we perform least-squares fits to the bright Es and faint early-type galaxies separately. We partition the bright Es from the other early-type galaxies with the dotted line at $M_R \geq -22.17$ mag. The dashed line represents a most recent $L \propto \sigma^n$ from the literature (Forbes, & Ponman 1999), where $\log \sigma = -0.102M_B + 0.243$, corresponding to $n = 3.92$. We obtained the ordinary least squares fit (OLS, as described by Feigelson, & Babu 1992) for all the galaxies excluding bright Es. The dash-dot line represents the fit which minimizes the residuals in M_R , the dash-dot-dot minimization in $\log \sigma$, and the solid line is the bisector line. The details of the fits are summarized in Table 2. Only the galaxy with a very large observational error from MLKC02 (see Figure 4) is excluded from the linear regression.

Another diagnostic diagram used for the characterization of the low luminosity early-type galaxies and a comparison of their properties to those of the bright Es is the $C - \sigma$ relation. Figure 5 shows the Johnson B–R mag (from Trenham, unpublished data) vs. $\log \sigma$ for galaxies in our sample, including some galaxies with σ measurements from the literature. In case of the galaxies in common with the literature, we performed a weighted average on the velocity dispersions and their errors. We plot only galaxies that have $B - R$ measurements, except in the case of the Hudson *et al.* (2001) sample where we have derived the colours from the GMP catalogue. The transformation between the GMP $b - r$ colours and $B - R$ of our sample was: $B - R = (1.128 \pm 0.098)(b - r)_j - 0.535 \pm 0.178$. The derived $C - \sigma$ relations minimizing residuals in either $\log \sigma$, $B - R$, or using the bisector for all the galaxies in the figure are found in Table 3. The right-hand panel includes galaxies from clusters observed by Faber *et al.* (1989) where we used the colour transformation $(B - R) = (B - V) + 0.71$ from Fukugita, Shimasaku & Ichikawa (1995).

5 DISCUSSION

5.1 L- σ Relation for Faint Early-type Galaxies

Faber & Jackson (1976) showed that luminosity of bright Es correlates well with velocity dispersion (σ) for these galaxies. The $L - \sigma$, or Faber-Jackson, relation can be expressed as $L \propto \sigma^n$, where n was originally ≈ 4 (Faber & Jackson 1976; Sargent *et al.* 1977; Schechter & Gunn 1979; Schechter 1980; Tonry & Davis 1981; Terlevich *et al.* 1981). Tonry (1981) was the first to note a slight change of slope in the $L - \sigma$ relation suggesting that $n \approx 4$ for more luminous objects while $n \approx 3$ for fainter galaxies. This result was confirmed by Davies *et al.* (1983) who found $n = 4.2 \pm 0.9$ for galaxies brighter than $M_B = -20$ ($M_R < -21.67$) and $n = 2.4 \pm 0.9$ for those fainter than this magnitude, and Held *et al.* (1992) who found $n = 2.5$ for dEs.

Unfortunately, the data samples of Tonry (1981), Davies *et al.* (1983) and Held *et al.* (1992) only included a dozen of the faint early-type galaxies. To further investigate the

$L - \sigma$ relation for a wide range of luminosities we present a sample of 143 galaxies with $-22 \lesssim M_R \lesssim -17.5$ mag.

The $L - \sigma$ relation (Figure 4) derived for this large sample exhibits a change of slope; the slope of faint early-type galaxies is shallower than that of bright ellipticals. Following the results of previous studies and including these in our data set we find that the value of $n \sim 4$ fits the bright E end of the diagram. In contrast to bright Es, we obtain $L \propto \sigma^{2.01 \pm 0.36}$ for faint early-type galaxies (adopting the bisector fit). This relation spans a range of 4.5 magnitudes fainter than $M_R = -22.17$ mag, the lower limit of bright Es, and is the largest sample of the faint early-type galaxies in a single cluster thus far. Our result derived for 143 galaxies is consistent with $L \propto \sigma^{2.4 \pm 0.9}$ derived by Davies *et al.* (1983) for their 14 faint ellipticals and that of De Rijcke *et al.* (2004), and it is inconsistent with the standard Faber-Jackson relation. This raises intriguing questions concerning the physical processes responsible for the change of slope in the $L - \sigma$ relation.

We note that our galaxies exhibit a small systematic offset depending on their SNR, as discussed in section 3.2. However, if corrected for this effect of ~ 6 percent at the lowest σ and lowest SNR galaxies, the slope of the faint early-type galaxies would be even shallower than derived in this paper.

A feasible explanation of the different slope between bright Es and faint early-type galaxies may be due to the presence of other types of galaxies at lower luminosities. We used the photometry of Gutiérrez *et al.* (2004) to classify galaxies from the present combined sample. In cases where the bulge-to-total (B/T) luminosity ratios from Gutiérrez *et al.*'s data were unreliable, we used the NASA/IPAC Extragalactic Database (NED). We defined galaxies with $B/T = 1.0$ as bulge-dominated, $0.5 < B/T < 1.0$ as bulge+single exponential component galaxies, and $B/T < 0.5$ as single exponential component. This notation is to avoid confusion of calling galaxies with exponential light profiles strictly as disk galaxies, since dEs tend to have exponential profiles (see GG03). The distribution of these galaxies in the $L - \sigma$ plot (Figure 4, right) indicates that there is a slight difference in the slopes for each type. Although a different $L - \sigma$ relation can be derived for each galaxy type, the individual relations are still within 3σ of each other (Table 2). It is not surprising that a significant number of single exponential component galaxies appear to be present in this sample since this light profile best describes the dwarf elliptical galaxies. However, classifying these low-luminosity galaxies is difficult without resolved photometry and we also note discrepancies in classification depending on the literature source. Nonetheless, the slopes of all three galaxy types, single exponential component, bulge+exponential component and bulge-dominated galaxies, are still in disagreement with the FJ relation, but consistent with $L \sim \sigma^{2.01 \pm 0.36}$ as derived earlier for the low-luminosity early-type galaxies.

Tonry (1981) attributed the change of slope in the $L - \sigma$ relation to less luminous systems having significant rotation. Subsequently, Davies *et al.* (1983) investigated rotational properties of about a dozen faint Es with $-20.5 < M_B < -18$ mag ($-22.17 < M_R < -19.67$ mag), and showed that the faint Es rotate more rapidly than most of the bright Es. More recent studies of the low-luminosity early-type galaxies, i.e. Simien, & Prugniel (2001), Geha, Guhathakurta,

& van der Marel (2003), and van Zee, Skillman, & Haynes (2004) indicate that some of these objects have a rotational component while others show little or no rotation.

We investigate whether rotational effects in the faint early-type galaxies can cause the change of slope in the $L - \sigma$ relation using the following approach. We assume that there is a universal relation between the luminosity and the kinetic energy per unit mass (or KE) such as: $L \propto KE^2$, which is common to both faint early-type galaxies and bright ellipticals. Since the kinetic energy per unit mass for a spheroid is (from Busarello, Longo & Feoli 1992):

$$KE = \frac{1}{2}\langle v^2 \rangle = \frac{1}{2}V_{rot}^2 + \frac{3}{2}\sigma^2$$

the assumed universal relation between luminosity and kinetic energy per unit mass translates into a correlation between luminosity, σ , and the anisotropy parameter (V_{rot}/σ):

$$L = a\sigma^4 \left(\frac{V_{rot}^2}{\sigma^2} + 3 \right)^2$$

For bright ellipticals, the existence of the Faber-Jackson relation ($L = b\sigma^4$) implies that $V_{rot} = 0$, as it is indeed the case since bright ellipticals are anisotropy-supported stellar systems and show no or little rotation. For faint early-type galaxies, however, the existence of a relation such as $L = c\sigma^2$, implies that there is a systematic increase in the anisotropy parameter (i.e., in the amount of rotation) as the velocity dispersion (or luminosity) decreases:

$$\frac{V_{rot}^2}{\sigma^2} = \sqrt{\frac{c}{b}} \frac{1}{\sigma} - 3$$

This expression yields the amount of rotation a faint early-type galaxy would need to have in order to follow the same relation between luminosity and $\langle v^2 \rangle$ followed by bright Es. Under these assumptions, the observed change of slope in the $L - \sigma$ diagram would simply be the result of not including the rotational component in the kinematic energy of faint early-type systems.

Using the expression above we can calculate the expected V_{rot}/σ for galaxies at different luminosities and velocity dispersions, and compare them to the observed values. We show this comparison through a set of graphs (see Figure 6). The left panel shows V_{rot}/σ vs. M_R , and the right panel V_{rot}/σ vs. σ . The solid line in both panels represents the predicted value for V_{rot}/σ , while the points are the most recent data from the literature (Davies *et al.* 1983; Simien & Prugniel 2002; Pedraz *et al.* 2002; Geha, Guhathakurta & van der Marel 2003; van Zee, Skillman, & Haynes 2004).

According to the predicted relation between the V_{rot}/σ and M_R , V_{rot}/σ would have to increase steadily toward the faint end (left panel of Figure 6). For example, a faint early-type galaxy with $M_R = -18$ mag and $\sigma = 39 \text{ km s}^{-1}$ would have $V_{rot}/\sigma = 3.2$, or $V_{rot} = 123 \text{ km s}^{-1}$. This value seems unreasonably large when compared to observed V_{rot}/σ values from Geha, Guhathakurta & van der Marel (2003), which range from as low as 0.01 to ~ 0.5 . The discrepancy is worse for the faintest galaxies. We conclude that the predicted V_{rot}/σ is inconsistent with observations of early-type galaxies fainter than $M_R = -20.5$ mag. Therefore, it is implausible that rotation is solely responsible for the difference in the $L - \sigma$ slope between faint early-type and bright elliptical galaxies.

An independent confirmation of $L \propto \sigma^2$ has recently

been provided by De Rijcke *et al.* (2004). They investigate how well different galaxy formation scenarios reproduce this slope difference between the bright ellipticals and bulges of spirals and dEs. The semi-analytical models which include quiescent star formation, post-merger star-bursts and gas-loss triggered by supernova winds seem to describe this effect well.

Next, we address the scatter around the $L - \sigma$ relation for the faint early-type galaxies. The rms scatter of the bi-sector line is 0.52 mag, where 0.22 mag can be attributed to the observational errors, assuming $\delta M_R = 0.1$ mag. The scatter in the $L - \sigma$ relation of faint early-type galaxies is, therefore, intrinsic. A possible reason for this scatter could be that the faint early-type galaxies in question are not yet relaxed. This could indicate that in their recent history these galaxies have encountered interactions with other galaxies in the cluster. It is also possible that the age of the galaxy could have an effect on the scatter, as investigated by Forbes, & Ponman (1999). We do not have direct age measurements for these objects yet. However, in the following section we plot the colour- σ relation for our galaxies. Under assumptions described in the following section we are able to investigate the effects age and metallicity have on this relation.

In conclusion, faint early-type galaxies follow a well-defined $L \propto \sigma^{2.01 \pm 0.36}$ relation. This relation is distinct from the traditional Faber-Jackson relation defined for bright E galaxies and might indicate that bright Es should no longer be viewed as canonical early-type galaxies. We also conclude that rotation in the faint early-type galaxies is not responsible for the change in the slope relative to that derived for bright Es.

5.2 Colour- σ Relation

The colour-magnitude relation (CMR) is a well established relation for early-type galaxies. It is characterized by the more luminous galaxies displaying redder colours. This relation was investigated by many authors in the past who determined that the slope of the relation arises because the more massive galaxies are redder and more metal rich than the less massive galaxies (e.g., Terlevich, Caldwell, & Bower 2001, and references therein). Caldwell (1983) and Prugniel *et al.* (1993) found that faint early-type galaxies roughly follow the CMR for bright Es. A similar, distance-independent, relation is the correlation between colour and σ , $C - \sigma$.

In Figure 5, we show the $C - \sigma$ relation for faint early-type galaxies and bright ellipticals. All of the galaxies seem to follow the same relation, although we note the lack of bright Es in the plot containing only Coma galaxies (left panel). We confirmed the uniformity of the $C - \sigma$ relation by checking our result with the U-V colours of Terlevich, Caldwell, & Bower (2001). The right panel includes galaxies from different clusters (Faber *et al.* 1989) and indicates that both faint and bright early-type galaxies follow the same $C - \sigma$ relation.

Since luminosity and σ are related, the $C - \sigma$ relation is equivalent to the CMR, which in turn suggests a more fundamental relation between galaxy metallicity and mass. Although colours depend both on metallicity and age changes in the stellar populations, the evidence so far supports that metallicity changes are responsible for the slope of the CMR, while age differences contribute to the scatter

observed around that relation. In the following analysis we assume that the same applies to the $C - \sigma$ relation. Note however, that it is likely that both age and metallicity affect the slope and the scatter. Bernardi *et al.* (2005) show that galaxies with large velocity dispersion tend to be older. They also show that at a specific σ , galaxies have a wide range in both age and metallicity in a way that the older galaxies have smaller metallicities and the younger galaxies larger metallicities. Assuming that the intrinsic scatter in the $C - \sigma$ relation is predominantly due to age, it is possible to constrain the age variations at a given formation epoch for faint early-type galaxies.

Bower, Lucey and Ellis (1992) (hereafter BLE92) showed that it is possible to determine minimum ages for galaxies with different formation scenarios by implementing evolutionary stellar population synthesis models and the intrinsic scatter in the CMR of these galaxies. We closely follow their method but use the intrinsic scatter derived from the $C - \sigma$ relation for our galaxies instead. Since the uncertainty in the observed parameters is 0.024 mag, the intrinsic scatter is 0.067.

We used the evolutionary stellar population synthesis models of Bruzual, & Charlot (2003) to simulate a galaxy with an exponentially declining star-burst, $\tau = 1$ Gyr, and a Chabrier IMF. In Figure 7, top panel, we show how the $B - R$ colour of a galaxy with metalicity $Z = 1$ or $0.4 Z_\odot$ evolves with time. Hence, we find how the rate of change of colour varies with the age of the galaxy (middle panel). The colour change can be related to the intrinsic scatter in the colour and the range of epochs for major star-formation events by the relation:

$$\sigma_{(B-R)} = \frac{d(B-R)}{dt} \times \sigma_{SFE} \quad (1)$$

where $\sigma_{(B-R)}$ is the scatter in $B - R$ colour and σ_{SFE} is the range in the star formation epoch (BLE92). This is in accordance with the assumption that the scatter in $C - \sigma$ is only due to age variation, or in this case, to the scatter in the star formation epoch.

After finding the $d(B-R)/dt$ at different ages of the galaxy, and using the intrinsic scatter of 0.067 in the $C - \sigma$ relation, we derive values for the maximum range in the star formation epoch. In Figure 7 (bottom panel) we show the maximum range in the star formation epochs as a function of the formation time, constrained by the intrinsic scatter in $C - \sigma$ for our sample. If the average age of our galaxy sample is 10 Gyr old, for example, the maximum range in its star formation epoch will be ~ 3 Gyr. However, in order to determine the upper limit on variations in the ages of galaxies we must take into account that the scatter in the SF epoch will also depend on how the galaxies were formed. Different formation scenarios can be parametrised by a parameter β , which describes the degree of coordination of galaxies during their formation. BLE92 define β as ‘the ratio of the spread in formation time to the characteristic time-scale at formation,’ where the galaxy formation times range as $\beta(t_H - t_F)$ (t_H is the age of the universe, and t_F is the time of formation of the galaxy). For example, $\beta = 1$ for uncoordinated galaxy formation, and $\beta = 0.1$ for strong coordination. Assuming solar metallicity, the minimum average age for the faint early type galaxies in our sample with $\beta = 0.1$ is ~ 6 Gyr (Figure 7, middle panel) with a scatter in the star for-

mation epoch of ± 1 Gyr (where $t_H = 13.7$ Gyr, $\Omega_M = 0.3$ and $\Omega_\Lambda = 0.7$). As a reference, a galaxy that is 6 Gyr old must have formed at redshift $z \sim 0.7$. Note that we can only put a lower limit on the ages of galaxies and an upper limit on the scatter in their SF epoch, provided that we know the level of coordination of galaxies during their formation.

Although we initially assumed that the scatter of the $C - \sigma$ relation is due to an age spread around the formation epoch in a single burst, secondary bursts of star formation will also contribute to the scatter. In fact, observations of galaxies in clusters at redshifts $z \sim 0.5$ point to a possibility of secondary star-bursts (Butcher & Oemler 1978; Butcher & Oemler 1984) in what may become today's population of faint early-type galaxies in clusters. By modeling the secondary star-bursts, we can place upper limits on the starburst strengths.

Assuming that all galaxies formed at $t > 10$ Gyrs and had a secondary starburst ~ 5 Gyrs ago, we again use the models of Bruzual, & Charlot (2003) with two exponentially declining bursts to make this constraint. For this purpose we also follow the discussion of BLE92. Using the scatter in the $B - R$ colour for various uniformly distributed burst strengths, solar metallicity and a Chabrier IMF, we find the typical rms burst strength $r_{typ} = \Delta(B - R)/0.17$ (the ratio between the stellar mass of the secondary burst to that of the initial burst). Our observed scatter of $(B - R)_{rms} = 0.07$ places an upper limit on the secondary burst of 40 percent by stellar mass of the first burst. Unfortunately, this constraint is not very robust since it strongly depends on the assumptions of the age of the starburst and the modeling components.

In conclusion, we have shown that there is a well defined relation between colour and σ for faint early-type systems. Assuming that metallicity changes are responsible for the slope of this correlation while age variations are the main contributor to the scatter, it is possible to constrain the age range of major star formation events for a given formation epoch. However, it is difficult to decouple the effects of age and metallicity using colours. In future papers we will study the detailed stellar population properties of faint early-type galaxies, both age and metallicity, using line strength indices and stellar population synthesis models. Furthermore, we will test if the galaxies in the centre of the cluster are more metal-rich than those in the outskirts, since this is predicted by the galaxy harassment model (Moore, Lake, & Katz 1998).

6 SUMMARY

We present velocity dispersion measurements for 69 faint early-type galaxies in the centre of the Coma cluster with $-22.17 \lesssim M_R \lesssim -17.5$ mag. We derive the $L - \sigma$ relation for faint early-type galaxies as $L \propto \sigma^{2.01 \pm 0.36}$, which differs from the Faber-Jackson relation, $L \propto \sigma^4$, defined for bright ellipticals. Rotation in these objects is investigated as a possible cause for the difference in the slope. Although rotation may contribute to the scatter in this relation, it is not the main cause for the different slope derived for these galaxies.

We also investigate whether the slope change is due to the presence of different classes of early-type galaxies in our sample. Although our sample includes bulge-dominated,

bulge+single exponential component and a few single exponential component galaxies, all three types essentially follow the same relation.

We find that faint early-type galaxies follow a well-defined $C - \sigma$ relation. By assuming that this relation is mostly driven by an increased metallicity with increasing galaxy mass, while the scatter reflects age differences, we investigated how we can constrain either the ages, the range of star formation epoch, or the strength of secondary bursts for the faint early-type galaxies for various galaxy formation scenarios.

ACKNOWLEDGMENTS

We thank our referee, Michael Hudson, for his suggestions which have significantly improved a previous version of this paper. We also thank Alister Graham for many insightful discussions, Javier Gorgas, Nicolás Cardiel and Patricia Sánchez-Blázquez for help and instructions on velocity dispersion measurements; Marla Geha for an independent check of velocity dispersions measurements; Neil Trentham for providing the B-R colours for our galaxies; Eric McKenzie for discussions and help with stellar synthesis models; Nicolas Gruel for help and use of his catalogue cross-correlation program; and Nelson Caldwell for providing the U-V colour catalog. R. G. acknowledges funding from the archive HST proposal HF01092.01-97A. R.G. also thanks the Yale TAC for generous allocation of time on the WIYN telescope.

REFERENCES

Bender, R., Burstein, D., & Faber, S. M., 1992, ApJ, 399, 462
Bender, R., & Nieto, J. L., 1990, A&A, 239, 97
Bernardi, M., Renzini, A., da Costa, L.N., Wegner, G., Alonso, M.V., Pellegrini, P.S., Rit, C., Willmer, C.N.A., 1998, ApJL, 508, 143
Bernardi, M., Sheth, R. K., Nichol, R. C., Schneider, D. P., & Brinkmann, J., 2005, AJ, 129, 61
Binggeli, B., Sandage, A., & Tarenghi, M., 1984, AJ, 89, 64
Bower, R.G., Lucey, J.R., & Ellis, R.S., 1992, MNRAS, 254, 601
Brodie, J. P., & Huchra, J. P., 1991, ApJ, 379, 157
Bruzual, G., & Charlot, S., 2003, MNRAS, 344, 1000
Busarello, G., Longo, & Feoli, A., 1992, A&A, 262, 52
Butcher, H., & Oemler, A. Jr., 1978, ApJ, 219, 18
Butcher, H., & Oemler, A. Jr., 1984, ApJ, 285, 426
Caldwell, N., 1983, AJ, 88, 804
Caldwell, N., 1987, AJ, 94, 1116
Caldwell, N., & Bothun, G. D., 1987, AJ, 94, 1126
Capaccioli, M., Caon, N., & C'Onofrio, M. 1992, MNRAS, 259, 323
Cardiel, N. 1999, Dissertation, *Star formation in Central Cluster Galaxies*, Univ. Complutense, Madrid
Colless, M., Dalton, G., Maddox, S., Sutherland, W., Norberg, P., Cole, S., Bland-Hawthorn, J., Bridges, T., Cannon, R., Collins, C., and 19 coauthors, 2001, MNRAS, 328, 1039

Colless, M., & Dunn, A.M., 1996, *ApJ*, 458, 435

Davies, R.L., Efstathiou, G., Fall, M., Illingworth, G., & Schechter, R.L., 1983, *AJ*, 266, 41

de Carvalho, R. R., & Djorgovski, S., 1992, *ApJ*, 389, 49

De Rijcke, S., Dejonghe, H., Zeilinger, W. W., Hau, G. K. T., 2001, *ApJL*, 559, 21

De Rijcke, S., Michielsen, D., Dejonghe, H., Zeilinger, W. W., & Hau, G. K. T., 2004, *astroph* 0412553, v2

de Vaucouleurs, G., 1948, *Ann. d' Astrophys.*, 11, 247

Faber, S. M., & Jackson, R. E., 1976, *ApJ*, 204, 668

Faber, S. M., & Lyn, D. N. C., 1983, *ApJ*, 266, 17

Faber, S. M., Wegner, G., Burstein, D., Davies, R., Dressler, A., Lynden-Bell, D., & Terlevich, R. J., 1989, *ApJS*, 69, 763

Feigelson, E. D., & Babu, G. J., 1992, *AJ*, 397, 55

Ferguson, H. C., & Binggeli, B., 1994, *A&A Rev.*, 6, 67

Ferguson, H.C., & Sandage, A., 1988, *AJ*, 96, 1520

Forbes, D.A., & Ponman, T.J., 1999, *MNRAS*, 309, 623

Fukugita, M., Shimasaku, K., & Ichikawa, T., 1995, *PASP*, 107, 945

Geha, M., Guhathakurta, P., & van der Marel, R., 2002, *AJ*, 124, 3073

Geha, M., Guhathakurta, P., & van der Marel, R., 2003, *AJ*, 126, 1794

Gorgas, J., Pedraz, S., Guzmán, R., Cardiel, N., & González, J. J., 1997, *ApJ*, 481, 19

González-González, J. J., 1993, Dissertation, *Line-Strength Gradients And Kinematic Profiles in Elliptical Galaxies*, UC Santa Cruz

Goodwin J., G., Metcalf, N., & Peach, J., V., (1983)

Graham, A. W., & Guzmán R., 2003, *AJ*, 125, 2936

Graham, A. W., 2004, *ApJ*, 613L

Gutiérrez, C. M., Trujillo, I., Aguerri, J. A., Graham, A. W., & Caon, N., 2004, *ApJ*, 602, 644

Guzmán, R., Graham, A. W., Matković A., Vass, I. Gorgas, J., & Cardiel, N., 2003, *ASP Conference Series*, *The Fundamental Properties of Dwarf Elliptical Galaxies in Clusters*

Held, E. V., & Mould, J. R., 1994, *AJ*, 107, 1307

Held, E. V., de Zeeuw, T., Mould, J., & Picard, A., 1992, *AJ*, 103, 851

Hudson, M. J., Lucey, J. R., Smith, R. J., Steel, J., 1997, *MNRAS*, 291, 488

Hudson, M. J., Lucey, J. R., Smith, R. J., Schlegel, D. J., & Davies, R. L., 2001, *MNRAS*, 327, 265

Jørgensen, I., Franx, M., & Kjærgaard, P., 1995, *MNRAS*, 276, 1341

Jerjen, H., & Binggeli, B., 1997, in *ASP Conf. Ser.* 116, *The Nature of Elliptical Galaxies*, ed. M. Arnaboldi, G. S. Da Costa, & P. Saha (San Francisco: ASP), 239

Jerjen, H., Binggeli, B., & Freeman, K. C., 2000a, *AJ*, 119, 593

Karachentsev, I.D., Karachentseva, V.E., Richter, G.M., & Vennin, J.A., 1995, *Astronomy and Astrophysics*, 296, 643

Kormendy, J., 1985, *ApJ*, 295, 73

Mehlert, D., Noll, S., Appenzeller, I., Saglia, R. P., Bender, R., Böhm, A., Drory, N., Fricke, K., Gabasch, A., Heidt, J., and 6 coauthors, 2002, *A&A*, 393, 809

Mobasher, B., Bridges, T. J., Carter, D., Poggianti, B. M., Komiyama, Y., Kashikawa, N., Doi, M., Iye, M., Okamura, S., Sekiguchi, M., Shimasaku, K., Yagi, M., & Yasuda, N., 2002, *ApJS*, 137, 279

Moore, B., Lake, G., & Katz, N., 1998, *ApJ*, 495, 139

Moore, B., Lake, G., & Katz, N., 1996, *IAU Circ.*, 171, 203

Moore, S. A., Lucey, J. R., Kuntschner, H., & Colless, M., 2002, *MNRAS*, 336, 382

Pedraz, S., Gorgas, J., Cardiel, N., Sanchez-Blazquez, P., Guzmán, R., 2002, *MNRAS*, 332, L59

Peterson, R. C., & Caldwell, N., 1993, *AJ*, 105, 1411

Peterson, R. C., & Caldwell, N., 1983, *AJ*, 105, 1411

Prugniel, Ph, Bica, E., Klotz, A., & Alloin, D., 1993, *A&AS*, 98, 229

Sandage, A., & Binggeli, B., 1984, *AJ*, 89, 919

Sargent, W. L. W., Schechter, P. L., Boksenberg, A., & Shortring, K., 1977, *ApJ*, 212, 326

Schechter, P. L., & Gunn, J. E., 1979, *ApJ*, 229, 472

Schechter, P. L., 1980, *AJ*, 85, 801

Simien, F., & Prugniel, P., 2002, *A&A*, 384, 371

Smith, R.J., Hudson, M.J., Nelan, J.E., Moore, S.A., Quinn, S.J., and 6 co-authors, 2004, *AJ*, 128, 1558S

Terlevich, A. I., Davies, R. L., Faber, S. M., & Burstein, D., 1981, *MNRAS*, 196, 381

Terlevich, A. I., Caldwell, N., & Bower, R. G., 2001, *MNRAS*, 326, 154

Tonry, J.L., 1981, *ApJ*, 251, 1

Tonry, J.L., & Davis, M., 1981, *ApJ*, 246, 680

van Zee, L., Skillman, E.D., & Haynes, M.P., 2004, *AJ*, 128, 121

Wirth, A., & Gallagher, J. S., 1984, *ApJ*, 282, 85

Table 1. Table of σ measurements

GMP No.	Galaxy Name	RA h:m:s	Dec. $^{\circ} \ ' \ "$	b_j mag	V_r km s^{-1}	δV_r km s^{-1}	σ km s^{-1}	$\delta\sigma$ km s^{-1}	SNR
(1)	(2)	(3)	(4)	(5)	(6)	(7)	(8)	(9)	(10)
2478		13:00:45.46	27:50:06.00	18.09	8670.5	2.0	50.0	5.1	28
2489		13:00:44.69	28:06:00.70	16.69	6539.1	1.3	93.8	2.3	54
2510		13:00:42.92	27:57:45.49	16.13	8336.9	2.0	126.7	2.5	48
2516	IC 4042	13:00:42.85	27:58:14.90	15.34	6321.3	3.6	176.2	4.6	46
2519		13:00:42.65	28:06:56.90	18.68	6107.0	26.5	71.2	76.5	13
2529		13:00:41.28	28:02:40.74	18.63	8519.6	2.1	42.3	5.5	28
2535	IC 4041	13:00:40.94	27:59:46.19	15.93	7026.9	2.0	123.8	2.4	47
2541	NGC 4906	13:00:39.83	27:55:24.40	15.44	7436.6	3.9	176.6	4.0	45
2585		13:00:35.50	27:56:32.15	18.44	6898.7	2.6	29.6	6.3	23
2603		13:00:33.45	27:49:25.60	17.36	8099.9	1.6	53.7	4.7	39
2654		13:00:28.06	27:57:19.75	16.38	6940.7	2.5	142.7	3.5	51
2676		13:00:26.24	28:00:30.17	19.03	5527.8	6.7	48.9	18.8	10
2692		13:00:24.90	27:55:34.14	18.20	7866.3	2.7	41.4	5.6	26
2778		13:00:18.88	27:56:11.75	16.69	5260.6	1.5	56.8	3.9	34
2784		13:00:18.62	28:05:48.01	18.36	7739.8	6.3	63.8	7.5	15
2799		13:00:17.72	27:59:13.29	18.70	5968.0	4.4	44.6	9.4	17
2805		13:00:17.11	28:03:48.29	16.57	6103.7	2.1	128.9	2.5	48
2839	IC 4021	13:00:14.83	28:02:26.93	16.01	5720.8	2.6	160.0	2.8	53
2852		13:00:13.72	27:52:00.28	17.80	7327.5	1.8	41.5	3.0	27
2861		13:00:12.98	28:04:30.05	16.26	7455.4	1.8	123.2	2.3	53
2879		13:00:11.23	28:03:53.16	18.05	7270.6	2.5	43.8	5.2	23
2912	NGC 4895A	13:00:09.20	28:10:11.73	16.07	6713.3	2.7	149.9	2.8	54
2917		13:00:08.50	27:57:15.23	19.13	6212.6	7.0	51.8	13.1	12
2922	IC 4012	13:00:08.10	28:04:41.15	15.93	7185.7	3.6	185.1	4.2	45
2929		13:00:07.56	27:57:27.22	18.66	6178.2	6.7	22.4	15.5	13
2940	IC 4011	13:00:06.48	28:00:13.19	16.08	7182.8	2.9	126.3	4.2	45
2960		13:00:05.47	28:01:26.46	16.78	5847.6	1.6	68.7	2.4	45
2985		13:00:03.83	27:57:51.31	17.87	5310.7	4.8	43.1	10.2	15
3017		13:00:01.05	27:56:41.80	17.91	6790.9	4.7	58.5	12.2	22
3018		13:00:01.08	27:59:27.80	19.31	7476.1	21.0	75.7	71.2	11
3034		12:59:59.56	27:56:24.42	18.06	6106.0	26.0	169.4	84.4	9
3058		12:59:57.72	28:03:52.35	17.71	5791.0	2.8	38.0	7.8	23
3068		12:59:56.75	27:55:46.40	16.47	7646.6	2.2	106.3	2.9	44
3073	NGC 4883	12:59:56.10	28:02:03.43	15.43	8054.0	3.8	173.3	5.2	45
3098		12:59:54.03	27:58:12.05	18.63	6740.7	7.3	59.2	35.0	14
3121		12:59:51.53	28:04:22.80	17.34	7405.6	3.0	49.8	6.2	24
3126		12:59:51.08	27:49:56.68	17.55	7826.1	2.1	53.7	3.8	26
3131		12:59:50.26	27:54:43.52	18.68	7195.5	5.0	49.9	8.5	13
3133		12:59:50.18	27:55:27.65	17.23	9674.8	2.0	79.6	3.0	35
3166		12:59:47.03	27:59:29.02	18.37	8315.3	5.1	58.8	8.0	16
3170	IC 3998	12:59:46.88	27:58:24.04	15.70	9302.1	2.2	142.6	4.2	41
3196		12:59:44.77	27:53:21.47	18.35	6747.3	3.9	55.0	10.3	19
3201	NGC 4876	12:59:44.47	27:54:43.02	15.51	6657.0	2.8	169.7	3.6	45
3205		12:59:44.30	27:52:01.98	17.61	6203.7	3.3	56.8	3.5	25
3206		12:59:44.29	27:57:28.36	16.36	6856.5	2.1	79.6	3.3	33
3209		12:59:44.25	28:00:45.14	19.37	7097.4	7.6	66.5	14.2	15
3213		12:59:43.80	27:59:39.15	16.14	6636.4	3.4	138.7	5.1	48
3222		12:59:42.38	27:55:27.37	16.47	6866.2	3.8	163.6	4.1	41
3254		12:59:40.36	27:58:03.95	16.57	7520.9	3.0	100.5	4.9	28
3269		12:59:39.73	27:57:12.57	16.12	7947.8	2.2	98.5	2.7	38
3292		12:59:38.08	28:00:01.79	17.70	4954.9	2.6	63.8	6.0	22
3296		12:59:38.00	27:54:24.64	15.88	7922.5	3.5	179.8	4.0	49
3312		12:59:37.09	28:01:05.15	18.68	7156.1	3.3	46.5	8.4	25
3313		12:59:37.06	27:49:31.05	17.53	6191.3	1.9	85.2	2.9	49
3336		12:59:35.58	27:54:19.86	18.47	6954.3	3.3	52.3	5.1	19
3339		12:59:35.37	27:51:47.40	17.54	6261.5	2.1	58.5	4.4	33
3340		12:59:35.25	27:56:03.28	18.54	4496.2	18.2	63.0	48.8	11
3352	NGC 4872	12:59:34.22	27:56:47.18	14.79	7120.1	4.3	211.1	6.4	42
3367	NGC 4873	12:59:32.86	27:58:59.55	15.15	5804.8	3.6	178.9	3.5	45

Table 1. *ctd.* Table of σ measurements

GMP No.	Galaxy Name	RA h:m:s	Dec. $^{\circ} \ ' \ ''$	b_j mag	V_r km s^{-1}	δV_r km s^{-1}	σ km s^{-1}	$\delta\sigma$ km s^{-1}	SNR
(1)	(2)	(3)	(4)	(5)	(6)	(7)	(8)	(9)	(10)
3376		12:59:32.19	27:55:14.35	18.24	7041.4	11.5	46.4	27.3	11
3400	IC 3973	12:59:30.90	27:53:01.74	15.32	4696.2	4.0	216.5	4.9	51
3438		12:59:28.60	28:01:07.71	19.01	5942.2	4.1	32.7	10.9	15
3471		12:59:26.67	27:59:52.73	16.45	6629.2	1.8	86.5	2.5	49
3486		12:59:25.41	27:56:02.48	17.73	7522.7	2.1	57.2	2.7	32
3510	NGC 4869	12:59:23.42	27:54:39.71	14.97	6791.6	3.9	195.5	4.5	46
3534		12:59:21.51	27:58:23.01	17.20	5994.6	1.2	53.5	2.9	43
3554		12:59:20.28	28:04:25.70	17.20	7091.3	1.5	62.6	3.2	43
3561	NGC 4865	12:59:19.87	28:05:01.70	14.54	4499.2	3.7	214.5	3.5	58
3565		12:59:19.79	27:58:22.80	18.44	7172.6	3.6	46.4	12.5	15
3625		12:59:15.91	27:53:07.67	19.63	6521.8	15.4	108.3	24.3	8
3629		12:59:15.66	27:53:55.19	19.03	5219.2	13.8	44.6	28.2	5
3645		12:59:14.71	27:53:42.42	18.64	6367.3	2.9	69.4	7.7	25
3656		12:59:14.02	28:04:32.70	15.53	7729.2	2.5	142.1	4.6	53
3681		12:59:11.64	28:00:31.46	18.01	6818.4	3.0	64.2	5.4	21
3706	IC 3960A	12:59:09.73	27:52:00.86	17.61	6851.9	1.8	95.7	2.5	49
3707		12:59:09.53	28:02:25.56	17.76	7150.9	2.1	76.8	3.6	38
3733	IC 3960	12:59:08.04	27:51:16.13	15.85	6520.2	3.2	175.9	6.0	45
3739	IC 3957	12:59:07.58	27:46:02.22	15.88	6316.9	2.4	172.5	4.1	46
3761	IC 3955	12:59:06.11	27:59:46.65	15.57	7602.9	2.9	153.8	3.0	49
3780		12:59:04.87	28:02:59.94	17.89	7957.3	2.0	57.9	3.4	30
3782		12:59:04.73	27:54:37.90	16.55	6363.0	2.0	110.7	2.5	56
3792	NGC 4860	12:59:03.99	28:07:23.61	14.69	7844.4	6.1	256.9	7.2	41
3794		12:59:04.24	27:57:31.19	17.37	6952.6	2.5	130.0	3.1	47
3851		12:59:00.15	27:58:01.08	16.98	8233.8	1.8	83.2	2.7	41
3855		12:58:59.56	27:56:02.57	18.05	5702.7	4.7	49.7	5.9	22
3856		12:58:59.59	27:59:34.47	19.58	6186.7	32.0	122.8	37.4	8
3914		12:58:55.34	27:57:51.26	16.57	5650.6	3.7	161.1	3.6	46

Table 1: Notes.—Col.(1).—Galaxy number according to Goodwin, Metcalfe, & Peach (1983), (GMP from here on).

Col.(2).—NGC or IC name of galaxy.

Col.(3).—RA

Col.(4).—Dec

Col.(5).— b_j magnitude from the GMP catalogCol.(6).—Radial velocity, V_r .Col.(7).—Uncertainty in the radial velocity measurement, δV_r .Col.(8).—Velocity dispersion measurement, σ .Col.(9).—Uncertainty in the velocity dispersion, $\delta\sigma$.

Col.(10).—Signal-to-noise ratio of galaxies.

Table 2. $L - \sigma$ Least-Squares Fits

Galaxy Type (1)	Regression (2)	Intercept (3)	Slope (4)	rms (5)	n (6)
all galaxies	$M_R \mid \log \sigma$	-10.949 ± 0.375	-4.551 ± 0.180	0.510 mag	1.82 ± 0.07
all galaxies	$\log \sigma \mid M_R$	-8.846 ± 0.444	-5.585 ± 0.210	0.565 mag	2.23 ± 0.08
all galaxies	Bisector	-10.001 ± 0.376	-5.017 ± 0.179	0.521 mag	2.01 ± 0.07
Bulge-dominated	Bisector	-9.194 ± 0.565	-5.370 ± 0.269	0.653 mag	2.15 ± 0.11
Bulge+Exp. Comp.	Bisector	-11.374 ± 0.608	-4.370 ± 0.306	0.464 mag	1.75 ± 0.12
Exponential Comp.	Bisector	-12.021 ± 0.687	-4.101 ± 0.319	0.628 mag	1.64 ± 0.13

Table 2: Notes.–Col.(1).–Galaxy type in regression

Col.(2).–Regression order: $M_R \mid \log \sigma$, means minimizing in M_R on $\log \sigma$. In case of Single Exponential Component, Bulge+Single Exponential Component and Bulge-dominated galaxies we only show the bisector value (Figure 4, *right* pannel).

Col.(3).–Intercept and uncertainty in linear regression

Col.(4).–Slope and uncertainty in linear regression

Col.(5).–rms of points around the linear fit.

Col.(6).–The power n of $L \propto \sigma^n$.

Table 3. $C - \sigma$ Least Squares Fits

Panel	Regression	Intercept	Slope	rms
Left	$B-R \mid \log \sigma$	0.904 ± 0.045	0.323 ± 0.023	0.066 mag
	$\log \sigma \mid B-R$	0.435 ± 0.162	0.555 ± 0.081	0.066 mag
	Bisector	0.680 ± 0.089	0.434 ± 0.045	0.071 mag
Right	$B-R \mid \log \sigma$	1.007 ± 0.026	0.279 ± 0.011	0.049 mag
	$\log \sigma \mid B-R$	0.595 ± 0.080	0.463 ± 0.036	0.049 mag
	Bisector	0.807 ± 0.041	0.369 ± 0.018	0.052 mag

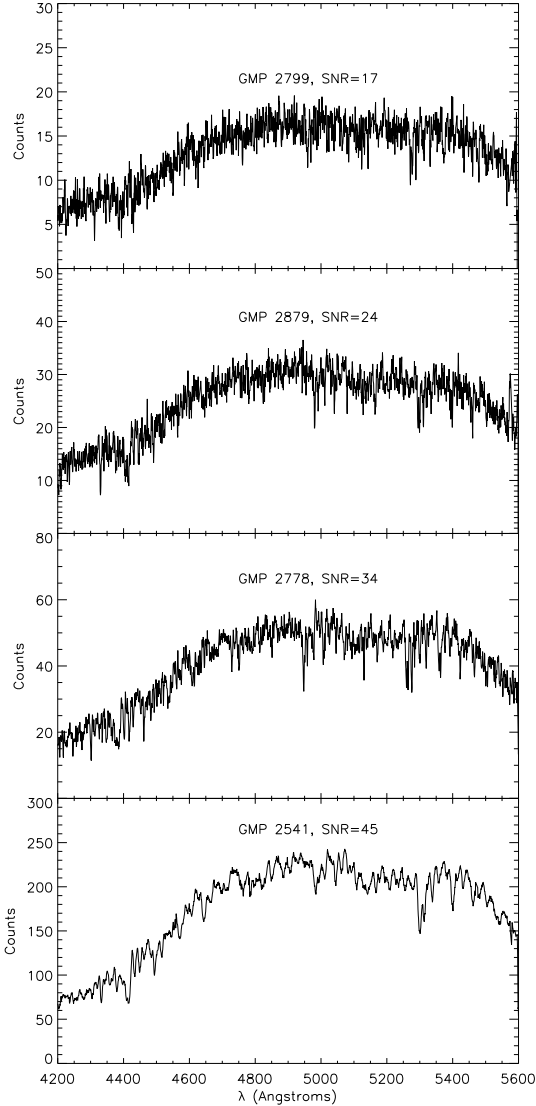


Figure 1. Spectra for early type galaxies of different luminosities. The GMP number (Goodwin, Metcalfe, & Peach 1983) and the signal-to-noise ratios (SNR) are given above each galaxy spectrum.

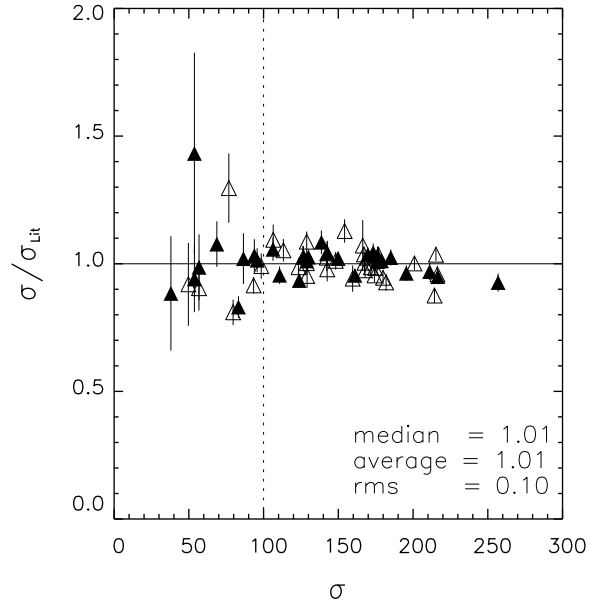


Figure 2. External check of σ measurements. The plot shows our σ measurements compared to NFPS (open triangles) and MLKC02 (solid triangles). The error bars in the $\sigma/\sigma_{\text{Lit}}$ are also shown.

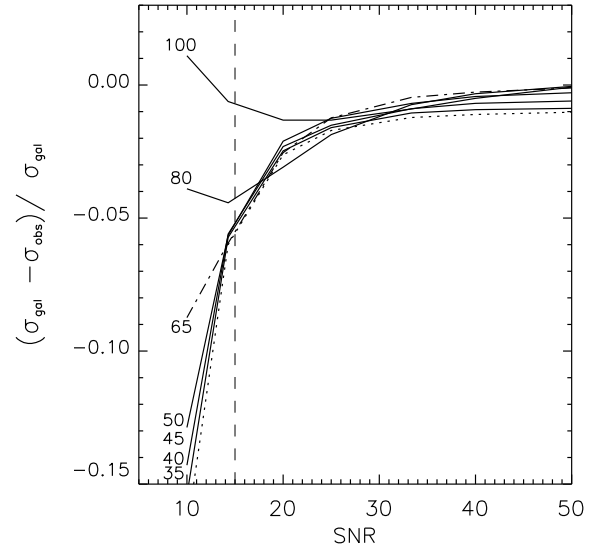


Figure 3. Systematic effects on σ measurements depending on the SNR of the galaxy. The y-axis shows the difference between the spectra with a given velocity dispersion, σ_{gal} , and the observed velocity dispersion, σ_{obs} , i.e. the same spectra with different amount of noise. The spectra were derived from simulations. The dotted line is for a spectrum of 35 km s^{-1} , while dash-dot line is for 65 km s^{-1} . The other lines are marked accordingly. We also included the dashed line at SNR of 15 as we chose this value as the upper limit for reliable σ measurements in this paper.

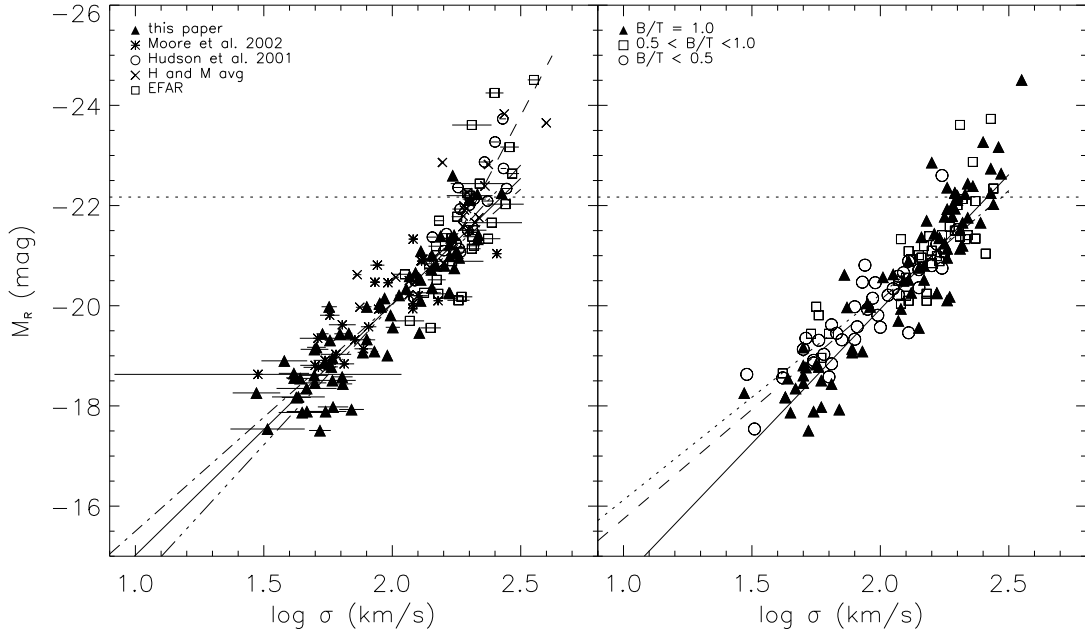


Figure 4. $M_R - \sigma$ plots for: (Left) All the Coma galaxies in our sample and those from the literature (see figure legend). The *dashed* line is the most recent FJ from literature, $L \propto \sigma^{3.92}$ (Forbes & Ponman, 1999); the *dash-dot* line is a least squares fit when minimising the residuals in M_R ; the *dash-dot-dot* when minimizing in $\log \sigma$; and the *solid* line is the bisector fit. (Right) Including only galaxies for which Gutiérrez *et al.* (2004) had the bulge-to-total ratio (B/T) measurements. The *solid* line is the least squares bisector fit for bulge-dominated (solid triangles), the *dashed* line for bulge+single exponential component (open squares), and the *dotted* line for single exponential component (open circles) galaxies.

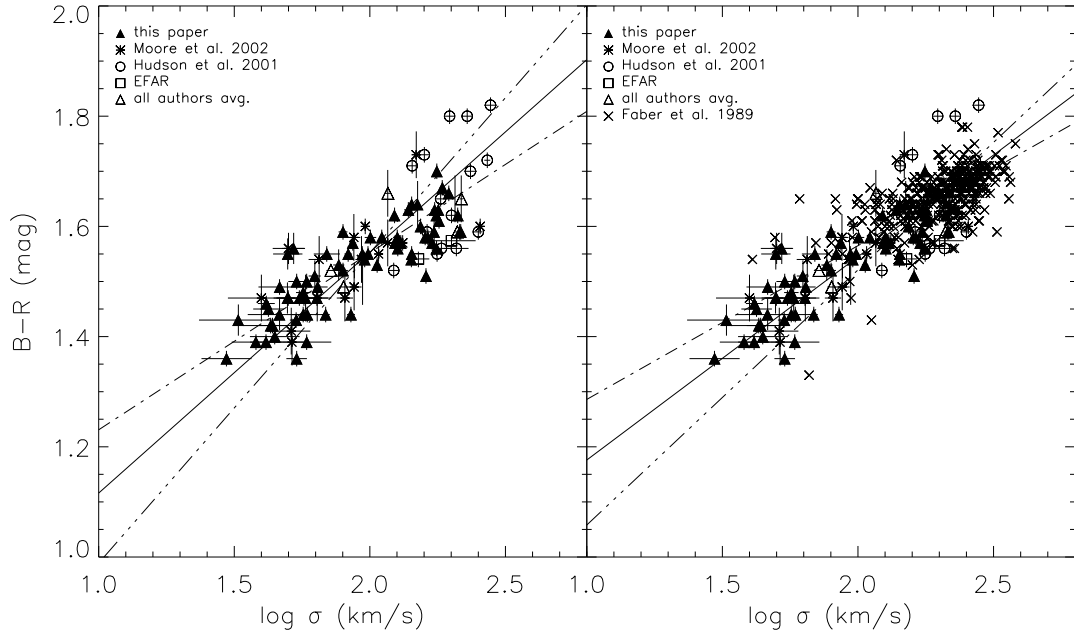


Figure 5. Colour – σ relation for early-type galaxies. In both panels the *dash-dotted* line represents a least squares linear fit when minimizing the residuals in $B-R$, *dash-dot-dot* when minimizing in $\log \sigma$, and the *solid* line is the bisector line. The *left* panel shows the $C - \sigma$ relation for the galaxies in the Coma cluster, while the *right* includes galaxies from all the clusters studied by Faber *et al.* (1989).

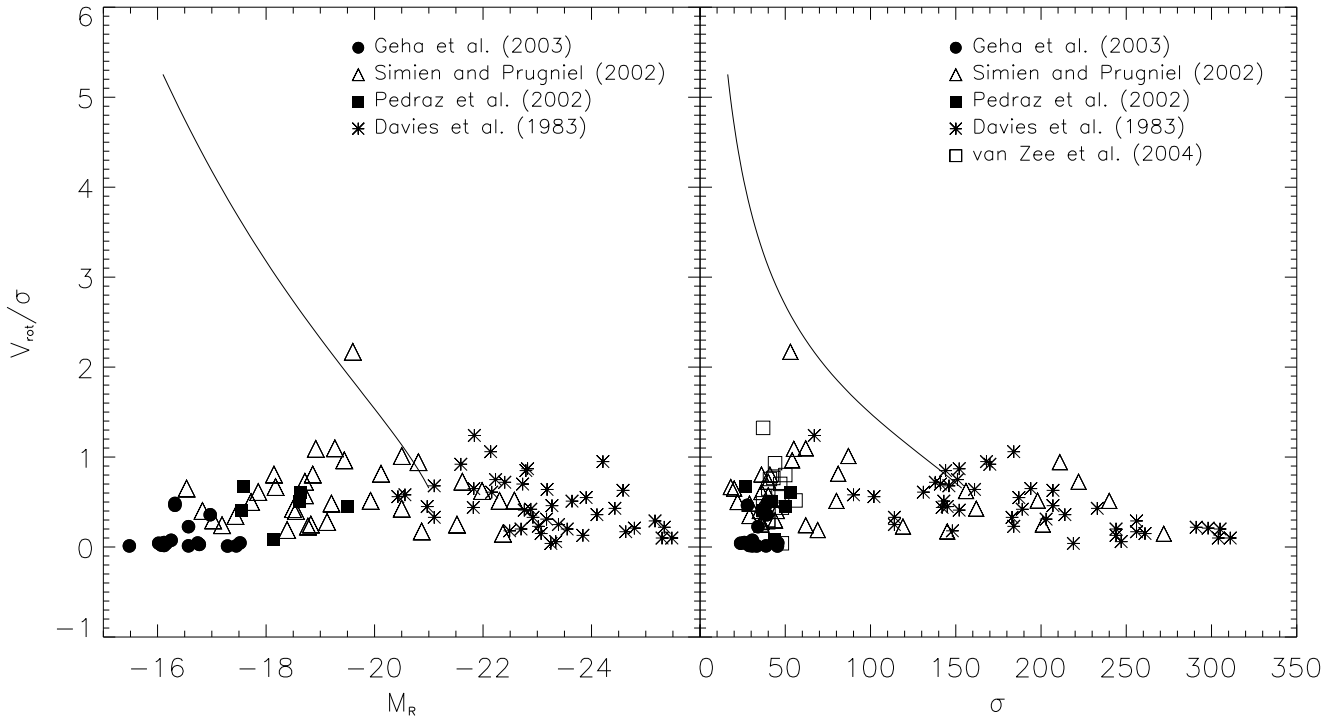


Figure 6. Comparison between observed and predicted relation V_{rot}/σ with M_R (Left) and σ (Right). In both panels the solid line represents the predicted V_{rot}/σ a galaxy would have to have in order for the faint early-type galaxies to follow the $L \propto \sigma^4$ relation defined for bright Es. The symbols are as shown in the figure legend.

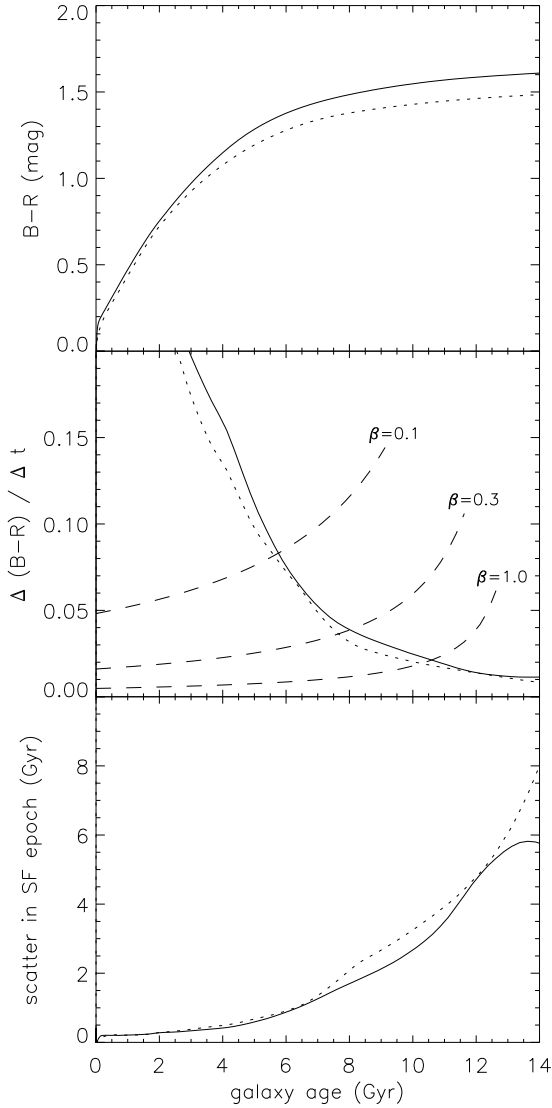


Figure 7. (Top) $B - R$ colour vs. galaxy age, assuming exponential burst. The *solid* line represents a galaxy with Z_{\odot} , while the *dotted* line is $0.4 Z_{\odot}$. (Middle) The rate of change of $B - R$ colour with time of formation. The *dashed* lines represent different β parameters which depend on how synchronized the galaxy formation is assumed to be. β of 1.0 corresponds to no coordination, while $\beta = 0.1$ is for strong coordination. (Bottom) Scatter in the star formation epoch vs. galaxy age. Assuming strong coordination in galaxy formation, the galaxy age of 6 Gyrs (from middle panel) would imply that its scatter in SF epoch is ~ 1 Gyr.

This paper has been typeset from a \TeX / \LaTeX file prepared by the author.